Electronic correlation and magnetic frustration in Li_2VOSiO_4 and $VOMoO_4$

Amin Kiani
Institute for Advanced Simulation, Forschungszentrum Jülich, 52425 Jülich, Germany

Eva Pavarini
Institute for Advanced Simulation, Forschungszentrum Jülich, 52425 Jülich, Germany
and JARA High-Performance Computing, RWTH Aachen University, 52062 Aachen, Germany

(Received 22 March 2016; revised manuscript received 15 June 2016; published 8 August 2016)

Li_2VOSiO_4 and $VOMoO_4$ have been proposed as realizations of the frustrated two-dimensional J_1-J_2 quantum Heisenberg model. In this work, in order to test this picture, we study their electronic and magnetic properties by using the local-density approximation + dynamical mean-field theory method. We calculate the magnetic linear response function starting from material-specific Hubbard models and systematically map our results onto those from generalized quantum Heisenberg models. We obtain the effective local magnetic moments and the associated magnetic exchange couplings, in particular the ratio J_2/J_1, a measure of the frustration degree, and the ratio $2J_\perp/(J_1+J_2)$, measuring the three-dimensionality degree. Our results support a weak frustration picture for both materials, with small but non-negligible long-range interplane couplings, leading to three-dimensional order at low temperature. Implications for the physics of the two systems are discussed.

DOI: 10.1103/PhysRevB.94.075112

I. INTRODUCTION

The layered vanadates Li_2VOSiO_4 and $VOMoO_4$ have been proposed as possible realizations of the two-dimensional J_1-J_2 quantum Heisenberg model, perhaps in the strong frustration regime [1–5]. The bonanza of unconventional phenomena predicted by theoretical studies of frustrated systems [6–10] has thus triggered a lot of attention towards these or similar materials [11–18], both theoretically and experimentally. From the point of view of the crystal and electronic structure Li_2VOSiO_4 and $VOMoO_4$ have several characteristics in common; they are both made by VO_5 pyramids forming layers; within a single layer, the VO_5 pyramids point alternately upwards and downwards (see Fig. 1), and the V atoms at the center of the pyramids form a squarelike lattice (see Fig. 2). Furthermore, they both have partially filled narrow V bands ($3d^1$ configuration). In the quantum Heisenberg model representation, the V atoms behave as local spins ($S = 1/2$); the magnetic exchange couplings J_1 and J_2 are those between V spins belonging to the same layer and forming a squarelike lattice; J_1 is associated with the V-V bond along the side of the square (at the center of pyramids pointing to opposite directions) and J_2 to the V-V bond along the diagonal.

The analysis of early experiments supported the strong frustration picture (with $J_1 \sim J_2$) [2,3]. For Li_2VOSiO_4, nuclear magnetic resonance (NMR), muon-spin rotation, and thermodynamic measurements lead to the estimates $J_1 + J_2 \sim 8.5$ K and $J_2/J_1 \sim 1.1$. Furthermore, these experiments suggest that a collinear antiferromagnetic structure is established around $T_N \sim 2.8$ K, a type of ordering predicted for the frustrated quantum Heisenberg model [19]. In such a magnetic structure—which in the rest of the paper will be called in short collinear—lines of parallel spins along, e.g., the **a** direction, are aligned antiferromagnetically with respect to each other. The corresponding ordered magnetic moments were estimated to be strongly reduced, $m(T \to 0) = 0.24\ \mu_B$ [2,3], a value again in agreement with the strongly frustrated quantum Heisenberg model picture. In line with this view, the lattice distortions observed around T_N were interpreted as frustration driven [2,3], with the degeneracy of the frustrated state perhaps lifted via the so-called spin Jahn-Teller effect [11–13]. Similar conclusions, although with sizably larger couplings, $J_1 + J_2 \sim 155$ K, and higher critical temperature, $T_N \sim 42$ K, were reached for $VOMoO_4$, for which it was estimated that $J_1 \sim J_2$ [4].

This is, however, not the end of the story. Indeed, the experiments discussed above do not probe J_2/J_1 directly, but only via the theoretical framework used in analyzing the data. In contrast to the strong frustration picture, *ab initio* studies [4,20,21] placed both systems in the weakly frustrated regime. As a matter of fact, these calculations, based on the local-density approximation (LDA) plus perturbation theory, yield $J_2/J_1 \sim 12$ for Li_2VOSiO_4 (well inside the collinear regime), and $J_2/J_1 \sim 0.2$ for $VOMoO_4$ (well inside the

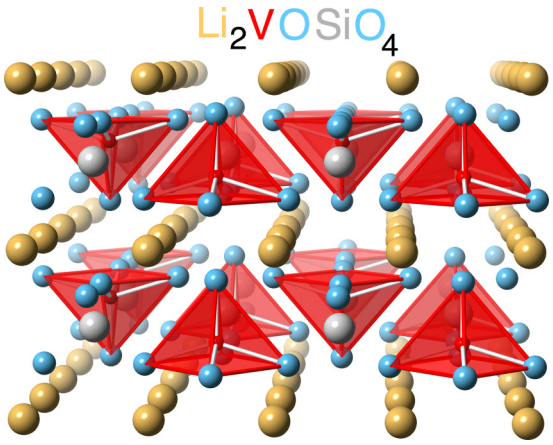

FIG. 1. The structure of Li_2VOSiO_4 showing the VO_5 pyramids arranged in layers. In a given layer, the V atoms at the center of pyramids form a pseudosquare lattice, with neighboring V^{4+} ions occupying positions $(1/4,1/4,z)$ and $(3/4,3/4,-z)$.

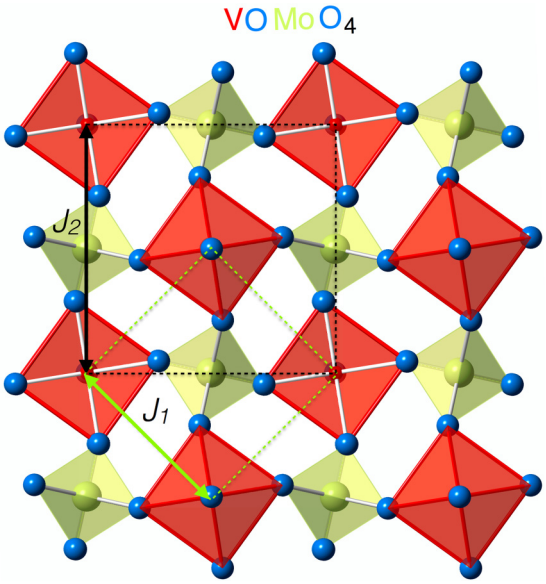

FIG. 2. The crystal structure of $VOMoO_4$ seen from the **c** direction, showing the pseudosquare lattice formed by VO_5 pyramids and MoO_4 tetrahedra. The coupling J_1 is between two V atoms at the center of nearest-neighboring pyramids pointing in opposite directions, while J_2 is between two V atoms at the center of next-nearest-neighboring pyramids, which point towards the same direction. Nearest-neighboring V^{4+} ions occupy the positions $(1/4,1/4,z)$ and $(3/4,3/4,-z)$. Differently than in Li_2VOSiO_4 (see Fig. 1), the VO_5 pyramids point away from the interior of the layer; furthermore, they are rotated.

Néel antiferromagnetic regime). Later on, a high-temperature expansion study of the J_1-J_2 Heisenberg model pointed out that the experimental specific heat and susceptibility of Li_2VOSiO_4 (from Refs. [2,3]) are compatible with large J_2/J_1 values in line with LDA-based results [5]. More recently, neutron diffraction and resonant x-ray scattering experiments have shown that both systems order magnetically in three dimensions [22,23], with critical temperatures close to previous estimates [2–4]: Li_2VOSiO_4 exhibits in-plane collinear antiferromagnetic order with ferromagnetic stacking along the **c** axis, $VOMoO_4$ Néel antiferromagnetic order below ∼40 K. Additionally, magnetic moments larger than previously estimated were reported [22,23], $m(T \to 0) \sim 0.63\ \mu_B$ for Li_2VOSiO_4 and $m(T \to 0) \sim 0.41\ \mu_B$ for $VOMoO_4$. These theoretical and experimental results, taken together, shift the balance in favor of a weak frustration scenario; the latter could explain a partial moment reduction [6–10].

Key to this conclusion is, however, to a large extent, the LDA estimate of the magnetic exchange couplings of the J_1-J_2 Heisenberg model. It becomes therefore crucial to put the latter to a test and study the emergence of effective local spins and the associated magnetic couplings both in a realistic setting and with a nonperturbative many-body method (beyond LDA and LDA+U). Indeed, the frustration degree could be either enhanced or suppressed by dynamical effects; reduced magnetic moments could, e.g., be partially associated with charge fluctuations; long-range exchange couplings could play a nontrivial role. To capture these effects it is essential to start from material-specific Hubbard models, rather than from effective J_1-J_2 Heisenberg models, solve them nonperturbatively and calculate the associated magnetic response functions and magnetic couplings. This is even more important in view of recent high-pressure studies and the associated LDA-based calculations of the magnetic couplings J_1 and J_2 [21]; they indicate that in Li_2VOSiO_4 increasing the pressure up to ∼7.6 GPa, leads to a decrease of about 40% of the J_2/J_1 ratio hinting to the possibility of tuning the ground state from collinear to disordered. Correlation effects might further help or hinder this possibility.

In the present paper we study the correlated electronic structure and the magnetic interactions in Li_2VOSiO_4 and $VOMoO_4$ by using the state-of-the-art approach, the local-density approximation plus dynamical mean-field theory (LDA+DMFT) method. To this end, the minimal material-specific many-body model to use is the half-filled one-band Hubbard model describing the xy low-energy states [24]. By using linear response-function theory on top of LDA+DMFT calculations we calculate the magnetic response function of the Hubbard model in the high-temperature ($T \gg T_N$) regime. This approach enables us to extract from the susceptibility both the effective local spin [25] S and the actual effective superexchange coupling $J(\mathbf{q})$, including nontrivial many-body effects; the Fourier transform of $J(\mathbf{q})$ to real space yields the couplings of a generalized quantum Heisenberg model. Our results identify superexchange driven magnetic instabilities at $q_C = (2\pi,0,0)$ for $VOMoO_4$ and $q_C = (\pi,\pi,\pi)$ for Li_2VOSiO_4. Apart from in-plane exchange couplings J_1 and J_2, the effective interlayer coupling $J_\perp$ could also play a role. We thus study both the ratio $2J_\perp/(J_1+J_2)$, a measure of the degree of three dimensionality, and the ratio J_2/J_1, a measure of the frustration degree. We find that they are weakly dependent on both U (in a very large interval) and the temperature. Overall, for a realistic $U \sim 5$ eV our results support for both systems the weak-frustration scenario with a small but non-negligible interplane coupling. The effective local spin S is very close to the ideal value $S = 1/2$, unless the ratio W/U becomes unrealistically large; this indicates that charge fluctuations are correspondingly small. Finally, we present a simple approximate analytical expression for the high-temperature magnetic LDA+DMFT susceptibility. This expression could be useful for analyzing magnetic instabilities in other frustrated Mott insulators; it can also be generalized to the multiband case.

The paper is organized as follows. In Sec. II we shortly present our implementation of the LDA+DMFT approach to calculate linear response functions. This implementation has been designed for systems described by a generalized Hubbard model and to optimally exploit the power of modern massively parallel supercomputers. In Sec. III we discuss our results for Li_2VOSiO_4 and $VOMoO_4$. In Sec. IV we present the conclusions. Technical details are provided in the Appendix.

II. METHOD

In order to study the magnetic properties of $VOMoO_4$ and Li_2VOSiO_4 we use the local-density approximation plus dynamical mean-field theory (LDA+DMFT) approach [28]. In a first step we build a generalized Hubbard Hamiltonian for

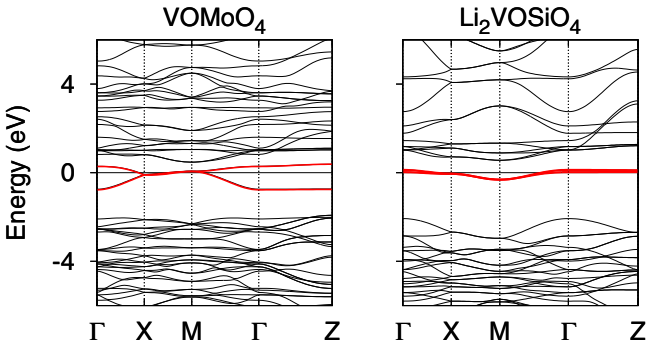

FIG. 3. Full LDA band structure of $VOMoO_4$ (left) and Li_2VOSiO_4 (right). The narrow xy band is the band crossing the energy zero.

the full set of the V d bands

$$H = -\sum_{ii'}\sum_{\sigma}\sum_{mm'} t_{mm'}^{ii'} c_{im\sigma}^{\dagger} c_{i'm'\sigma} + \frac{1}{2}\sum_{i}\sum_{\sigma\sigma'}\sum_{m(\neq m')} (U_{mm'} - J\delta_{\sigma\sigma'}) n_{im\sigma} n_{im'\sigma'} + \sum_{i}\sum_{m} U_{mm} n_{im\uparrow} n_{im\downarrow}, \quad (1)$$

where $c_{im\sigma}^{\dagger}$ ($c_{im\sigma}$) creates (annihilates) an electron with spin σ in orbital m on lattice site i and $n_{im\sigma} = c_{im\sigma}^{\dagger} c_{im\sigma}$. The parameters $U_{mm'} = U - 2J(1 - \delta_{mm'})$ and J are the screened direct and exchange Coulomb interaction, respectively. The elements of matrix $t_{mm'}^{ii'}$ are hopping ($i \neq i'$) and crystal-field ($i = i'$) integrals; we obtain them *ab initio* by downfolding to the V $3d$ bands and constructing a localized Wannier function basis; to do this we adopt the downfolding procedure based on the Nth-order muffin-tin orbital (NMTO) method. The full LDA band structure is shown in Fig. 3 [29]. For both $VOMoO_4$ and Li_2VOSiO_4 the $m = xy$-like band crosses the Fermi level and the remaining d bands are empty; the $m = xz, yz, x^2 - y^2$, and $3z^2 - r^2$ crystal-field states are well above the xy level. Thus for the actual dynamical mean-field theory (DMFT) [30] and cellular dynamical mean-field theory (cDMFT) calculations we proceed to further downfolding to the xy band; in the absence of experimental estimates of the gap and of measurements probing the spectral function, we perform the calculations varying U between 1 and 5 eV (see Fig. 4). In Sec. III C we will see that $U \sim 5$ eV is the value which best reproduces the Curie-Weiss temperature in both systems; it is also a typical value for vanadates [29]. We use both a Hirsch-Fye quantum Monte Carlo (QMC) [31] solver and a CT-HYB QMC quantum impurity solver [32], the latter in the implementation of Ref. [33]. The susceptibility calculations are mostly based on the Hirsch-Fye QMC code. Via the quantum-impurity solver we obtain $\chi^{\boldsymbol{\alpha}}(\boldsymbol{\nu})$, the Fourier transform of the local susceptibility tensor $\chi^{\boldsymbol{\alpha}}(\boldsymbol{\tau})$, defined as [34]

$$\chi^{\boldsymbol{\alpha}}(\boldsymbol{\tau}) = \langle \mathcal{T} c_{\alpha_1}(\tau_1) c_{\alpha_2}^{\dagger}(\tau_2) c_{\alpha_3}(\tau_3) c_{\alpha_4}^{\dagger}(\tau_4) \rangle - \langle \mathcal{T} c_{\alpha_1}(\tau_1) c_{\alpha_2}^{\dagger}(\tau_2) \rangle \langle \mathcal{T} c_{\alpha_3}(\tau_3) c_{\alpha_4}^{\dagger}(\tau_4) \rangle.$$

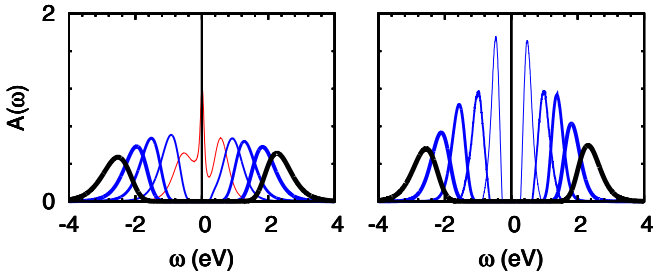

FIG. 4. LDA+DMFT spectral function for $VOMoO_4$ (left) and Li_2VOSiO_4 (right) at 380 K and for $1 < U < 5$ eV. The linewidth increases with increasing U in steps of 1 eV. The metal-insulator transition occurs for $VOMoO_4$ for U between 1.5 and 2 eV; instead, Li_2VOSiO_4 becomes insulator already between 0.5 and 1 eV.

Here $\mathcal{T}$ is the time order operator, $\boldsymbol{\tau} = (\tau_1, \tau_2, \tau_3, \tau_4)$ and τ_j are imaginary times. The indices $\boldsymbol{\alpha} = (\alpha_1, \alpha_2, \alpha_3, \alpha_4)$ and $\alpha_j = m_j \sigma_j i_j$ are collective orbital (m_j) spin (σ_j) and site (i_j) indices; the latter label, in cDMFT calculations, the V sites within the cluster $\{i_c\}$. The Fourier transform to Matsubara frequencies is $\chi^{\boldsymbol{\alpha}}(\boldsymbol{\nu}) = \chi^{\boldsymbol{\alpha}}_{n,n'}(\omega_m)$, where $\boldsymbol{\nu} = (\nu_n, -\nu_n - \omega_m, \nu_{n'} + \omega_m, -\nu_{n'})$, ν_n and $\nu_{n'}$ are fermionic and ω_m bosonic Matsubara frequencies. The tensor elements $\chi^{\boldsymbol{\alpha}}_{n,n'}(\omega_m) = [\chi(\omega_m)]_{N,N'}$ build a square matrix with elements $N = \alpha_1 n, \alpha_2 n$, $N' = \alpha_3 n', \alpha_4 n'$; for the magnetic susceptibility only terms with $\sigma_1 = \sigma_2 = \sigma$ and $\sigma_3 = \sigma_4 = \sigma'$ contribute. The $\chi(\omega_m)$ matrix is zero everywhere except within a quantum-impurity block ($i_j = i_1$ in DMFT and $i_j = \{i_c\}$ in cDMFT calculations); for clarity, we denote with N_c the elements N belonging to one of such blocks. The local susceptibility $\chi(\omega_m)$ calculated via QMC as discussed above, together with $\chi_0(\omega_m)$, the bubble contribution to the local susceptibility, a sum of product of Green function matrices, allows us to calculate the local vertex $\Gamma(\omega_m)$. This, in turn, yields, within the local-vertex-approximation, the lattice susceptibility $\chi(\mathbf{q}; \omega_m)$. Let us see how. In the local-vertex approximation [30,35] the lattice susceptibility $\chi(\mathbf{q}; \omega_m)$ is given by the solution of the Bethe-Salpeter equation

$$\chi(\mathbf{q}; \omega_m) = \chi_0(\mathbf{q}; \omega_m) + \chi_0(\mathbf{q}; \omega_m)\Gamma(\omega_m)\chi(\mathbf{q}; \omega_m). \quad (2)$$

Here $\chi(\mathbf{q}; \omega_m)$, $\chi_0(\mathbf{q}; \omega_m)$, and $\Gamma(\omega_m)$ are all $N \times N$ matrices; the elements of the matrix $\chi_0(\mathbf{q}; \omega_m)$ can be written as

$$[\chi_0(\mathbf{q}; \omega_m)]_{N,N'} = -\beta \delta_{nn'} \delta_{\sigma_2\sigma_3} \delta_{\sigma_1\sigma_4} \times \frac{1}{N_{\mathbf{k}}} \sum_{\mathbf{k}} G^{\mathbf{k}+\mathbf{q}}_{\alpha_2\alpha_3}(\nu_n + \omega_m) G^{\mathbf{k}}_{\alpha_4\alpha_1}(\nu_n), \quad (3)$$

where $G^{\mathbf{k}}_{\alpha_i\alpha_j}(\nu_n)$ is the (c)DMFT lattice Green function; thus, to calculate the lattice susceptibility it is sufficient to calculate the Green function matrix (we obtain it from the LDA Hamiltonian and the LDA+DMFT self-energy) and the local vertex matrix $\Gamma(\omega_m)$. The latter is the solution of the local Bethe-Salpeter equation [30,35]

$$\chi(\omega_m) = \chi_0(\omega_m) + \chi_0(\omega_m)\Gamma(\omega_m)\chi(\omega_m), \quad (4)$$

with

$$[\chi_0(\omega_m)]_{N_c,N_c'} = \frac{1}{N_{\mathbf{q}}} \sum_{\mathbf{q}} [\chi_0(\mathbf{q}; \omega_m)]_{N_c,N_c'}.$$

By solving Eq. (4) we find the expression of $\Gamma(\omega_m)$ in terms of the inverse of $\chi_0(\omega_m)$ and the inverse of $\chi(\omega_m)$; the latter is obtained, as we already discussed, directly from the QMC solution of the quantum-impurity problem. The local vertex, calculated in this way, is then replaced in Eq. (2), whose solution finally yields the lattice susceptibility tensor $\chi^{\alpha}_{n,n'}(\mathbf{q};\omega_m) = [\chi(\mathbf{q};\omega_m)]_{N,N'}$.

Finally, the magnetic susceptibility is given by

$$\chi(\mathbf{q};\omega_m) = \frac{(g\mu_B)^2}{4}\sum_{\alpha}(-1)^{\sigma_1+\sigma_3}\delta_{\sigma_1\sigma_2}\chi^{\alpha}(\mathbf{q};\omega_m)\delta_{\sigma_3\sigma_4},$$

where

$$\chi^{\alpha}(\mathbf{q};\omega_m) = \frac{1}{\beta^2}\sum_{nn'}\chi^{\alpha}_{n,n'}(\mathbf{q};\omega_m).$$

The bottleneck of the approach is the computation of the local or cluster susceptibility tensor with the quantum Monte Carlo method; this can be very time consuming, in particular in the multiorbital or multisite case, although the calculation is performed only once at the end of the self-consistency loop. To speed up the calculations we have parallelized our code optimizing it for modern massively parallel architectures. Furthermore, we directly sample with QMC the Fourier transform of the local Green-function matrix $G(\tau,\tau')$; we do this by shifting the discontinuities of the Green-function matrix to the border and using the two-dimensional Filon-trapezoidal method (see Appendix for more details), an approach which turned out to be very efficient. Finally, we perform the sum on the Matsubara frequencies for a finite number of frequencies and use an extrapolation procedure to recover the infinite number limit. Symmetries are exploited for further optimization.

III. RESULTS

A. Correlated electronic structure

Both $VOMoO_4$ and Li_2VOSiO_4 are characterized by narrow and well separated xy LDA bands at the Fermi level (see Fig. 3), with bandwidth $W \sim 1.1$ eV in the case of $VOMoO_4$ and sizably smaller, $W \sim 0.4$ eV in the case of Li_2VOSiO_4. For both systems the crystal field at the V site is octahedral in the first approximation. In the case of Li_2VOSiO_4 the crystal-field levels, taking the lowest as the energy zero, are (0,0.9,0.9) eV for the t_{2g}-like states and (2.25,2.4) eV for the e_g-like states. The main difference between the two systems is that $t_1 \sim 0.137$ eV in $VOMoO_4$ couples V between pyramids pointing away from the interior of the layer (see pattern for J_1 in Fig. 2); this hopping is negligible in Li_2VOSiO_4. The LDA hopping integral between neighboring pyramids in the same plane is t_2 (see pattern for J_2 in Fig. 2). We find that $t_2 \sim 0.033$ eV in $VOMoO_4$ and $t_2 \sim -0.037$ eV in Li_2VOSiO_4, i.e., its absolute value is comparable in the two materials; the hopping t_{1z} between V at the center of pyramids in first nearest-neighbor layers is also about the same in the two materials, with $t_{1z} \sim 0.012$ eV in $VOMoO_4$ and $t_{1z} \sim -0.010$ eV in Li_2VOSiO_4. The first next-nearest-neighbors hopping integral along $\mathbf{c}$ is $t_z \sim 0.012$ eV in $VOMoO_4$ and $t_z \sim 0.013$ eV in Li_2VOSiO_4, hence slightly less than one half of t_2 in both cases. Finally, t_{2z}, the hopping integrals between neighboring pyramids pointing in the same direction but belonging to neighboring layers, is about 5 meV in Li_2VOSiO_4 and even smaller in $VOMoO_4$.

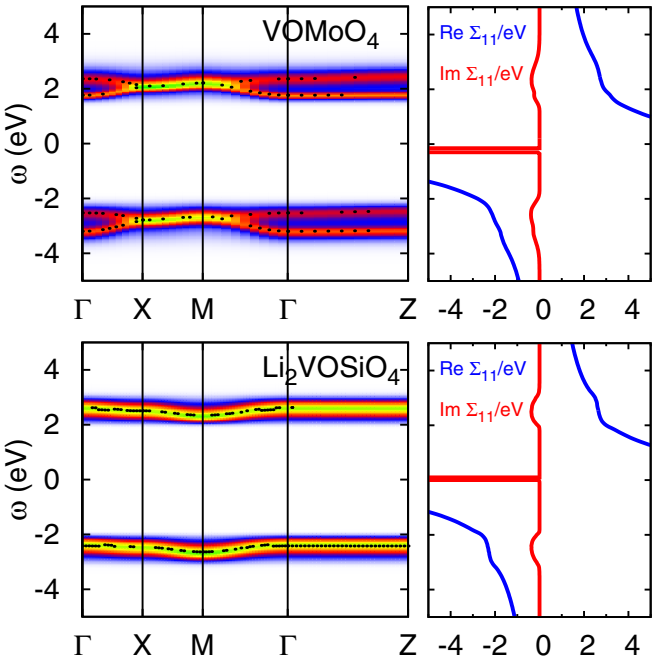

FIG. 5. Left: Correlated band structure of $VOMoO_4$ and Li_2VOSiO_4 for a realistic $U = 5$ eV, calculated at ~200 K. The dots are the poles of the Green function and yield the energy dispersion. The energy gap scales linearly with U. Right: Corresponding real-axis self-energy $\Sigma(\omega)$.

In the absence of an accurate experimental determination of the gap and, to the best of our knowledge, of experiments probing the spectral function, we calculate the correlated bands, the spectral function, the effective local spin, and the magnetic response function for several values of the screened Coulomb repulsion U. The spectral functions are shown in Fig. 4. We find that $VOMoO_4$ becomes an insulator for U between 1.5 and 2 eV, and Li_2VOSiO_4 for slightly smaller values, between 0.5 and 1 eV. Thus in the rest of the paper we focus on the range $2 < U < 5$ eV in particular. As we will see in Sec. III C, $U \sim 5$ eV yields Curie-Weiss temperatures in very good agreement with experiments for *both* materials; since $U \sim 5$ eV is also typical value for vanadates [29], we conclude that it is a realistic estimate for $VOMoO_4$ and Li_2VOSiO_4 as well. Experiments probing the gap and the spectral function could put this conclusion to a test. The correlated band structure for $U \sim 5$ eV is shown in Fig. 5, together with the corresponding self-energies on the real axis. The figure shows that the Hubbard bands exhibit the dispersion of the LDA bands.

B. Static magnetic susceptibility

Let us start with analyzing the case of $VOMoO_4$. The DMFT static magnetic susceptibility is shown in Fig. 6 for $U \sim 5$ eV and $T \sim 380$ K, well above T_N in the paramagnetic phase. Including the vertex correction turns out to be crucial. The $\chi_0(\mathbf{q};0)$ term alone is weakly temperature dependent; by analyzing our LDA+DMFT results we find that $\chi_0(\mathbf{q};0)$ is

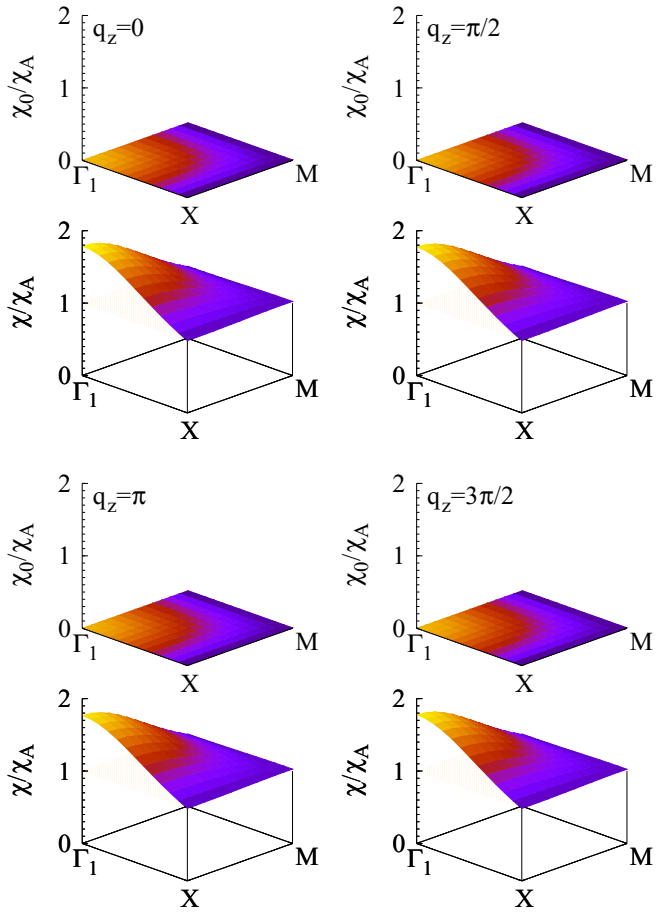

FIG. 6. $VOMoO_4$: Static magnetic susceptibility $\chi(\mathbf{q};0)/\chi_A(0)$ in the q_x,q_y plane for representative values of q_z, $T \sim 380$ K ($T \gg T_N$) and $U = 5$ eV; $\chi_A(0) \sim \mu_{\rm eff}^2/k_BT$ is the atomic susceptibility in the local spin (large βU) limit. For each value of q_z, the top panel shows the result without vertex correction and the bottom panel that with vertex correction. The special points in the q_x,q_y plane are $\Gamma_1 = (2\pi,0)$, $X = (\pi,0)$, and $M = (\pi,\pi)$.

approximately given by the expression obtained by replacing in the Green functions in Eq. (3) the self-energy with its atomic limit, with U renormalized by a factor r_0,

$$\Sigma(i\omega_n) \sim \frac{r_0^2U^2}{4}\frac{1}{i\omega_n}.$$

The factor r_0 can be obtained by fitting the actual self-energy. After performing analytically the Matsubara sums, we find, in the large βU limit (for more details see the Appendix)

$$\chi_0(\mathbf{q};0) \sim \frac{\mu_{\rm eff}^2}{U}\left[1 - \frac{1}{2U}\left(J_{r_0}(\mathbf{0}) + \frac{1}{2}J_{r_0}(\mathbf{q})\right)\right], \qquad (5)$$

where

$$J_{r_0}(\mathbf{q}) = (\chi_0(\mathbf{q};\mathbf{0}))^{-1} - (\chi_0(0))^{-1} = J_{\rm SPT}(\mathbf{q})/2r_0^2,$$

and $\mu_{\rm eff} = g\mu_B\sqrt{S(S+1)/3}$, where S is the effective local spin (for fully localized moments, $S = 1/2$). In this expression $J_{\rm SPT}(\mathbf{q})$ is the magnetic coupling obtained via many-body second-order perturbation theory, accounting, however, not only for J_1 and J_2 but also for long range exchange couplings. It is given by

$$J_{\rm SPT}(\mathbf{q}) \sim 4J_1\cos\frac{q_x}{2}\cos\frac{q_y}{2}\left[1 + 2\frac{J_{1z}}{J_1}\cos q_z + \left(\frac{J_{1z}}{J_1}\right)^2\right]^{1/2} + 2J_2(\cos q_x + \cos q_y) + 2J_z\cos q_z + 4J_{2z}(\cos q_x + \cos q_y)\cos q_z + \cdots, \qquad (6)$$

where $J_i \sim 4t_i^2/U$. For $VOMoO_4$ we find that the renormalization factor $r_0 \sim 1$. The expression Eq. (5) shows that $\chi_0(\mathbf{q};0)$ does not exhibit the Curie-Weiss temperature behavior associated with a local-moment system, and the effective magnetic exchange coupling extracted from $\chi_0(\mathbf{q};0)$ is about a factor 2 smaller than in second-order perturbation theory. The DMFT vertex correction has several effects. First, via the Bethe-Salpeter equation it enhances the susceptibility in a slightly nonuniform way. Then, it yields a high-temperature Curie-Weiss-like behavior, so that $\chi(\mathbf{q};0) \sim \mu_{\rm eff}^2/(T - T_{\mathbf{q}})$, where $T_{\mathbf{q}}$ is a generalized Curie-Weiss temperature. It follows from this that we can define the magnetic coupling as $J(\mathbf{q}) = -T_{\mathbf{q}}/\mu_{\rm eff}^2$. In first approximation we find $J(\mathbf{q}) \sim J_r(\mathbf{q})$ and the value of the renormalization factor is reduced from $r_0 \sim 1$ to $r \sim 0.7$. Thus our results show that for $VOMoO_4$, in first approximation, $J_r(\mathbf{q}) \sim J_{\rm SPT}(\mathbf{q})$. Furthermore, we find that the local susceptibility is close to the atomic magnetic susceptibility, and the effective static local vertex $\Gamma(0)$ is approximately given by

$$\Gamma(0) \sim \frac{1}{\mu_{\rm eff}^2}\left[U\left(1 + \frac{1}{2U}J_r(\mathbf{0})\right) - k_BT\right].$$

Remarkably, in the large temperature limit the r factor can be estimated expanding the Bethe-Salpeter equation (in the matrix form) around the atomic limit

$$\chi(\mathbf{q};0) \sim \chi_A(0) - \frac{r_0^2}{r^2}\,\chi_A(0)\,J_{r_0}(\mathbf{q})\,\chi_A(0),$$

where

$$\frac{r_0^2}{r^2} \sim \frac{1}{\beta^2}\sum_{nn'}\frac{[\chi_A(0)J_{r_0}(\mathbf{q})\chi_A(0)]_{n,n'}}{\chi_A(0)J_{r_0}(\mathbf{q})\chi_A(0)} \qquad (7)$$

and

$$\left[J_{r_0}(\mathbf{q})\right]_{n,n} = [(\chi_0(\mathbf{q};0))^{-1} - (\chi_0(0))^{-1}]_{n,n}.$$

The analytic expression of the atomic susceptibility matrix is given for completeness in the Appendix. This yields for $VOMoO_4$ a renormalization factor $r \sim 0.7$, close to the actual value obtained from fitting the DMFT data.

The susceptibility of Li_2VOSiO_4 is shown in Fig. 7. The conclusions are similar as for $VOMoO_4$; the susceptibility jumps from about zero without vertex correction to about 1 (in units of the atomic susceptibility) with vertex correction. The renormalization parameters are slightly larger than in $VOMoO_4$, $r_0 \sim 1.1$ and $r \sim 0.84$. For both Li_2VOSiO_4 and $VOMoO_4$ we find that at $\mathbf{q} = \mathbf{q}_X \equiv (0,\pi,\pi/2)$ the magnetic susceptibility $\chi(\mathbf{q}_X;0) \sim \chi_A(0) \sim \mu_{\rm eff}^2/k_BT$, indicating that $J(\mathbf{q}_X)$ is basically zero.

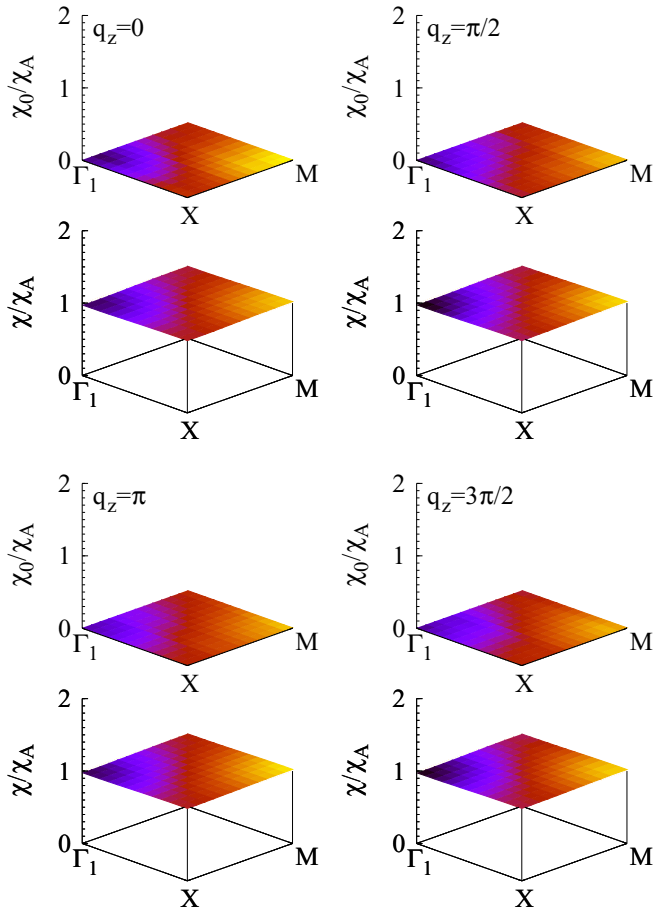

FIG. 7. Li_2VOSiO_4: Static uniform magnetic susceptibility $\chi(\mathbf{q};0)/\chi_A(0)$ in the q_x,q_y plane for representative values of q_z, $T \sim 380\,\mathrm{K}$ ($T \gg T_N$) and $U = 5\,\mathrm{eV}$; $\chi_A(0) \sim \mu_{\mathrm{eff}}^2/k_B T$ is the atomic susceptibility in the local spin (large βU) limit. For each value of q_z, the top panel shows the result without vertex correction and the bottom panel that with vertex correction. The special points in the q_x,q_y plane are $\Gamma_1 = (2\pi,0)$, $X = (\pi,0)$, and $M = (\pi,\pi)$.

C. Uniform Curie-Weiss temperature and effective magnetic moments

The inverse high-temperature susceptibility obtained with the LDA+DMFT approach exhibits a linear dependence on T in a wide temperature range, for all $\mathbf{q}$ (see Fig. 8 for $\mathbf{q} = \mathbf{0}$) and for a remarkably large set of U values. It is thus natural to define the actual Curie-Weiss temperature as $T_{\mathrm{CW}} = -T_0$. For $U \sim 5$ eV we find $T_{\mathrm{CW}} \sim 191$ K for $VOMoO_4$ and $T_{\mathrm{CW}} \sim 8$ K in Li_2VOSiO_4, in very good agreement with NMR measurements, 155 ± 20 K for $VOMoO_4$ [4] and 8.2 ± 1 K for Li_2VOSiO_4 [2,3]. This comparison confirms the strength of our approach. Next, we calculate the effective magnetic moment from the static magnetic susceptibility in the $T \to \infty$ limit, $\mu_{\mathrm{eff}} \sim \lim_{T\to\infty} \sqrt{(T + T_{\mathrm{CW}})\chi(0)}$, and also directly from the equal time correlation function matrix. The result obtained from the second approach is shown in Fig. 9. We find that for $U = 5$ eV in both systems this moment is quite close to $S = 1/2$, indicating that charge fluctuations are small for this (realistic) U value. Thus, if $U \sim 5$ eV, charge fluctuations do not reduce S enough to explain alone the small staggered magnetic moment m reported in neutron-scattering experiments [25]; they could however play a role if the gap was smaller (i.e., $U \sim 2$ eV). An experimental determination of the gap and the spectral function would be therefore desirable to reach the final conclusions. Interestingly we observe sizable effective local spins even deep in the (hypothetical) metallic regime, with $S \sim 0.436$ for $VOMoO_4$ for $U = 1$ eV, to be compared with $S \sim 0.498$ for $U = 5$ eV. For Li_2VOSiO_4 the

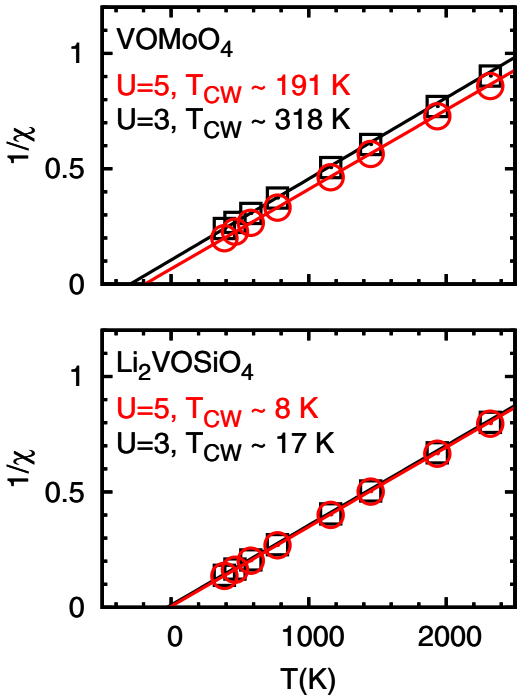

FIG. 8. Inverse uniform static magnetic susceptibility for $VOMoO_4$ and Li_2VOSiO_4. The lines are a least-square fit of the calculated points; the intersect with the temperature axis yields the Curie-Weiss temperature T_{CW}. For a realistic $U \sim 5$ eV we obtain $T_{\mathrm{CW}} \sim 191$ K for $VOMoO_4$ and 8 K for Li_2VOSiO_4. We find a linear behavior also for relatively small values of U.

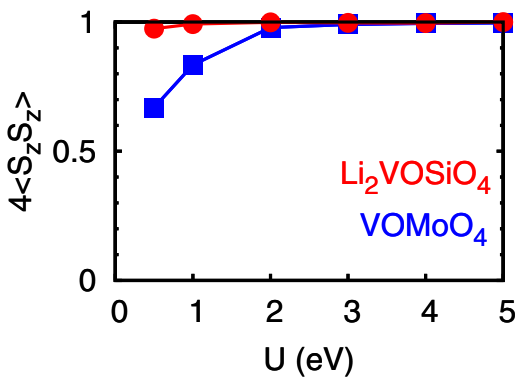

FIG. 9. Normalized local spin-spin correlation function $4\langle S_z S_z\rangle$ as a function of U; the points are calculated at ~200 K but change little when the temperature is raised to 380 K. The spin-spin correlation function yields the effective local spin S [25]; in particular, a local spin $S = 1/2$ corresponds to $4\langle S_z S_z\rangle = 1$. Squares: $VOMoO_4$; circles: Li_2VOSiO_4.

effective spin is $\sim 1/2$ in the whole range of U values because the system is on the verge of the metal-insulator transition already for $U \sim 0.5$ eV.

D. Magnetic superexchange couplings

As previously discussed, in first approximation we find that the LDA+DMFT magnetic coupling is given by $J(\mathbf{q}) \sim J_r(\mathbf{q})$. To a closer look nontrivial many-body effects partially modify also the $\mathbf{q}$ dependence. This can be understood from a reexamination of the approximate renormalization factor r_0^2/r^2 given in Eq. (7), which is, in principle, $\mathbf{q}$ dependent. Let us here focus on two aspects, the degree of two-dimensional frustration and the interlayer coupling. A measure of the degree of frustration is the ratio J_2/J_1. Since even in the general case the exchange coupling has an expansion of the type (6), ratio J_2/J_1 can be approximately written as

$$J_2/J_1 \sim -\frac{\chi(\mathbf{q}_M;0)^{-1} - \chi(\mathbf{q}_X;0)^{-1}}{\chi(\mathbf{q}_1;0)^{-1} + \chi(\mathbf{q}_2;0)^{-1} - 2\chi(\mathbf{q}_X;0)^{-1}},$$

where $\mathbf{q}_1 = (\pi/2,\pi/2,0)$, $\mathbf{q}_2 = (\pi/2,\pi/2,\pi)$, $\mathbf{q}_M = (\pi,\pi,\pi/2)$, and $\mathbf{q}_X = (0,\pi,\pi/2)$. We find that, in the full range $U \sim 2$–5 eV the ratio J_2/J_1 is weakly temperature dependent and only slightly U dependent, in line with the weak charge fluctuation picture and indicating that corrections beyond $O(U^{-1})$ are weak. In the case of $VOMoO_4$ for $U \sim 5$ eV we obtain $J_2/J_1 \sim 0.06$, a value close, but slightly larger than the ratio obtained via LDA and perturbation theory. For Li_2VOSiO_4 the value $J_2/J_1 \sim 10$ is partially reduced with respect the LDA value $J_2/J_1 \sim 12$. Such a 20% reduction is not sufficient to drive the system out of the weak frustration regime. It is worth noting, however, that such a change is comparable with the reduction reported in high-pressure studies up to 7.6 GPa on the basis of LDA calculations [21]. This indicates that it might be interesting to push the pressure even higher; everything else remaining the same, J_2/J_1 could move under pressure closer to the spin-liquid regime than it was previously estimated.

The actual phase transition to three-dimensional antiferromagnetic order crucially depends on the coupling between planes [36], hence it is important to study the degree of three dimensionality as well. Let us define the average interplane coupling as $J_\perp \sim \frac{1}{7}(J_z + 2J_{1z} + 4J_{2z})$ and the degree of three dimensionality as $f_\perp = 2J_\perp/(J_2 + J_1)$. The latter can be estimated as

$$f_\perp \sim -\frac{\chi(\Gamma;0)^{-1} - \chi(Z;0)^{-1}}{\chi(\mathbf{q}_M;0)^{-1} - \chi(\mathbf{q}_X;0)^{-1}} \frac{2J_2/J_1}{7(1 + J_2/J_1)},$$

where $Z = (0,0,\pi)$ and $\Gamma = (0,0,0)$. Remarkably, also $f_\perp$ is weakly temperature dependent. For both $VOMoO_4$ and Li_2VOSiO_4 the value of $f_\perp$ is slightly larger with respect to the LDA value. Furthermore, in the case of $VOMoO_4$ we find that $2J_{1z}$ and $J_z + 4J_{2z}$ are comparable, with $2J_{1z}$ slightly larger; instead, in Li_2VOSiO_4 we find that $2J_{1z}$ is smaller than the sum $J_z + 4J_{2z}$.

Finally, we investigated nonlocal effects on the exchange couplings via cellular DMFT (cDMFT), always in the $T \gg T_N$ limit. In particular, we perform two-sites cDMFT calculations, which should already give strong effects; we restore the full 3D periodicity of the original lattice on the susceptibility directly, at the end of the calculation. Remarkably, in the high-temperature regime, relevant to extract the effective exchange couplings, we find no sizable changes in $J(\mathbf{q})$, in the ratio J_2/J_1 or $2J_\perp/(J_2 + J_1)$. This is perhaps due to the fact that V sites have, despite of the layered structure, a relatively large coordination number. The overall effective coupling $J(\mathbf{q})$ is partially reduced with respect to single-site DMFT; this reduction is slightly larger in the case of $VOMoO_4$, with a reduction factor ~ 0.95.

Putting all our results together, our LDA+DMFT calculations support a weakly frustrated picture and magnetic order in three dimensions at low temperature. In $VOMoO_4$ the magnetic coupling $J(\mathbf{q})$ points to an instability at $\mathbf{q}_C = (2\pi,0,0)$, i.e., the Γ_1 point in the $q_z = 0$ panel of Fig. 6. This corresponds to Néel antiferromagnetic order in the **ab** plane and ferromagnetic stacking along the **c** axis ($2J_{1z} \gtrsim J_z + 4J_{2z}$). In Li_2VOSiO_4 the critical vector is $\boldsymbol{q}_C = (\pi,\pi,\pi)$, yielding collinear order in the **ab** plane and antiferromagnetic stacking along the **c** axis ($J_z + 4J_{2z} \gtrsim 2J_{1z}$). Thus, in the **ab** plane, the magnetic instabilities predicted via LDA+DMFT are in full agreement with those reported experimentally [22,23]; along **c**, instead, apparently neutron-scattering experiments [23] yield ferromagnetic stacking in Li_2VOSiO_4; this suggests that either the interplane ferromagnetic local Coulomb exchange dominates over superexchange, reversing the sign of $2J_{1z} - J_z - 4J_{2z}$, or that, most likely, the structural changes observed around T_N modify the relative weights of $2J_{1z}$ and $J_z + 4J_{2z}$. Since to the best of our knowledge no detailed structural data are yet available across the magnetic transition, we cannot identify which of the two mechanisms actually dominates [37].

IV. CONCLUSIONS

In this work we study the electronic and magnetic properties of two materials regarded as paradigmatic realizations of the square-lattice two-dimensional quantum Heisenberg model, Li_2VOSiO_4 and $VOMoO_4$. To do this we adopt the LDA+DMFT approach and its cluster extension. We calculate the magnetic susceptibility in the local-vertex approximation and in the high-temperature ($T \gg T_N$) regime. This enables us to calculate the effective magnetic moments and to extract the actual effective superexchange coupling $J(\mathbf{q})$, i.e., to systematically build the realistic quantum-Heisenberg model associated with the two systems. This approach yields Curie-Weiss temperatures in excellent agreement with experiments. For realistic values of U we find no sizable charge fluctuations and well defined $S \sim 1/2$ effective local moments. We derive a practical approximated expression for the local vertex and the susceptibility, which can be used to analyze other frustrated Mott insulators, and extended, e.g., to multiband systems. By analyzing our results for $J(\mathbf{q})$, we find that both systems are only partially well described by the quantum two-dimensional J_1-J_2 Heisenberg model; long-range couplings, in particular in the third dimension, play an important role. Our results support for both systems the weak frustration picture, with three-dimensional order below the critical temperature. This level of in-plane frustration, although weak, together with small long-range couplings, could alone explain (see, e.g., studies of the 2D Heisenberg models in Refs. [7–10]) the partial reduction of ordered magnetic moments observed via

neutrons scattering experiments [22,23]. In the **ab** plane, our calculations indicate collinear order for Li_2VOSiO_4 and Néel order for $VOMoO_4$, in line with neutron-scattering experiments. The delicate balance between the small but competing interactions along the **c** direction suggests that the layered vanadates are close to an effective zero coupling (or high frustration) in the third dimension ($2J_{1z} - J_z - 4J_{2z} \sim 0$); for this reason they behave as effectively two-dimensional systems in a wide temperature range. Structural distortions at T_N are likely to be essential to determining the actual type of stacking along the **c** axis. Finally, we point out the analogies of the low-energy electronic structure ($t - t'$ one-band model) of these layered vanadates with that of high-temperature cuprate superconductors [24]; in that view it would be interesting to study experimentally the effects of electron or hole doping.

ACKNOWLEDGMENTS

Calculations have been done on the JARA RWTH cluster and on the Jülich BlueGene/Q. We acknowledge financial support from the Deutsche Forschungsgemeinschaft through research unit FOR 1346.

APPENDIX

1. Fourier transform of $G(\tau',\tau'')$

To perform the Fourier transform of $G(\tau',\tau'')$, needed to calculate the local response function, we proceed as follows. We construct inside the QMC block a new Green function $\widetilde{G}(\tau+\tau'',\tau'')$, whose discontinuities are shifted on the boundaries, i.e., at $\tau = 0$ and $\tau = \beta$

$$\widetilde{G}(\tau+\tau'',\tau'') = \begin{cases} G(\tau+\tau'',\tau''), & \tau+\tau'' < \beta, \\ -G(\tau+\tau''-\beta,\tau''), & \tau+\tau'' \geqslant \beta, \end{cases}$$

where $\widetilde{G}$ is β periodic in τ'' and β antiperiodic in τ. The Fourier transform of G can be expressed as a function of $\widetilde{G}$ as follows:

$$\begin{aligned} G(\nu_n,\nu_{n'}) &= \iint d\tau' d\tau'' e^{i\nu_n\tau' - i\nu_{n'}\tau''} G(\tau',\tau'') \\ &= \iint d\tau d\tau'' e^{i\nu_n\tau + i(\nu_n-\nu_{n'})\tau''} \widetilde{G}(\tau+\tau'',\tau''), \end{aligned}$$

where the integrals are in the interval $[0,\beta]$. We calculate it by using the two-dimensional Filon-trapezoidal method [38,39]. We split the interval $[0,\beta]$ in L time slices $\tau_l = l\Delta\tau$ with $l = 0,\ldots,L$, $\Delta\tau = \beta/L$ and approximate the $\widetilde{G}(\tau+\tau'',\tau'')$ by a piecewise polynomial function in the interval $\tau \in [\tau_{l_1},\tau_{l_1}+\Delta\tau]$ and $\tau'' \in [\tau_{l_2},\tau_{l_2}+\Delta\tau]$,

$$\begin{aligned} \widetilde{G}(\tau+\tau'',\tau'') \sim\ & \widetilde{G}_{l_1,l_2} + (\tau-\tau_{l_1})\frac{\widetilde{G}_{l_1+1,l_2} - \widetilde{G}_{l_1,l_2}}{\Delta\tau} \\ & + (\tau''-\tau_{l_2})\frac{\widetilde{G}_{l_1,l_2+1} - \widetilde{G}_{l_1,l_2}}{\Delta\tau} \\ & + (\tau-\tau_{l_1})(\tau''-\tau_{l_2}) \\ & \times \frac{\widetilde{G}_{l_1+1,l_2+1} - \widetilde{G}_{l_1+1,l_2} - \widetilde{G}_{l_1,l_2+1} + \widetilde{G}_{l_1,l_2}}{\Delta\tau^2} \\ & + \cdots, \end{aligned}$$

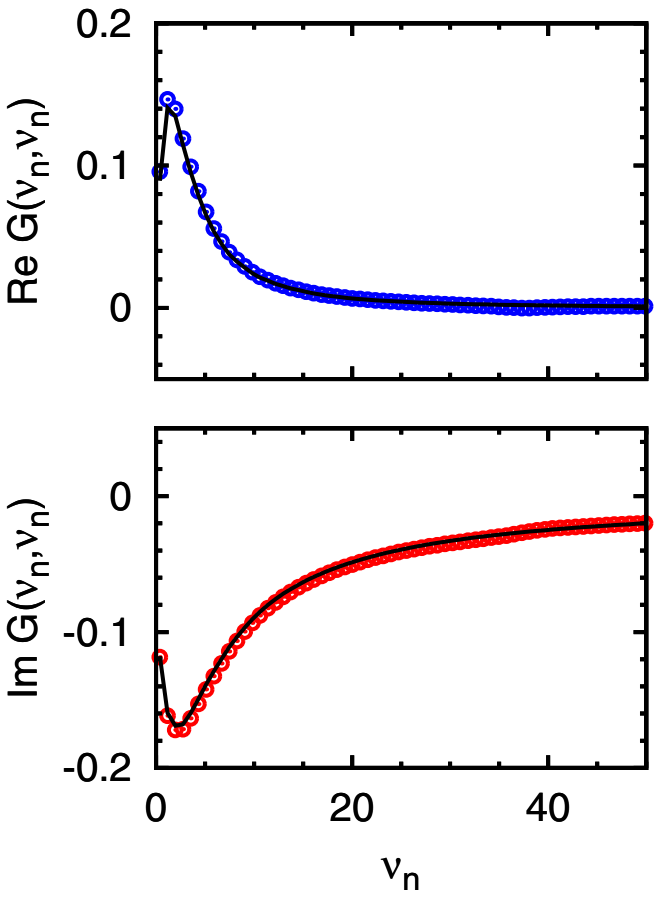

FIG. 10. Fourier transform of a typical Green function. Top: Real part. Bottom: Imaginary part. Full lines: Numerically exact Green function, calculated via a spline at the end of the QMC run. Open circles: Fourier transform of the Green function calculated after moving the singularities to the border and using then the Filon-trapezoidal method. These results are obtained for $\Delta\tau \sim 0.17$. The error remains less than 5% even for $\Delta\tau \sim 0.33$, twice as large.

where $\widetilde{G}_{l_1,l_2} = \widetilde{G}(\tau_{l_1}+\tau_{l_2},\tau_{l_2})$. Through this approximation

$$G(\nu_n,\nu_{n'}) \approx \sum_{l_1 l_2} w_{l_1}(\theta_1) w_{l_2}(\theta_2) e^{i(\nu_n-\nu_{n'})\tau_{l_2} + i\nu_n\tau_{l_1}} \widetilde{G}_{l_1,l_2},$$

where $\theta_1 = \Delta\tau\nu_n$, $\theta_2 = \Delta\tau(\nu_n - \nu_{n'})$ and

$$w_l(\theta) = \begin{cases} w_0(\theta) = \Delta\tau\left[\frac{1+i\theta-e^{i\theta}}{\theta^2}\right], & l = 0, \\ w_L(\theta) = w_0(-\theta), & l = L, \\ w_0(\theta) + w_L(\theta), & l \neq 0, L. \end{cases}$$

Thanks to the shift of the singularities to the border we automatically recover the proper limit at equal times

$$\widetilde{G}(\tau+\tau'',\tau'') \to \widetilde{G}(0^+,0),$$

as well as the correct $1/\nu_n$ decay of $G(\nu_n,\nu_n)$. This is shown in Fig. 10 for a test case. The Fourier transform based on the Filon-trapezoidal deviates from the exact result at $\nu_p = 2\pi M/\Delta\tau$, where M is an integer; the actual error decreases with increasing M. At these frequencies, for typical values of β/L, due to the prefactor $w_l(\theta_1)w_{l'}(\theta_2)$, the Green function $G(i\nu_n,i\nu_n)$ is already small even for $M = 1$.

2. Atomic susceptibility

The atomic magnetic susceptibility matrix for an idealized one-level atom is given by

$$\left[\frac{\chi_A(0)}{(g\mu_B S)^2}\right]_{n,n'} = M_{n'}\frac{dM_n}{dy} + M_n\frac{dM_{n'}}{dy} + \delta_{m,0}\beta n(-y)M_nM_{n'} - \beta n(y)[\delta_{n,n'} + \delta_{n,-n'}]\frac{dM_n}{dy} - \frac{1}{y}\{M_{n'} - \beta[n(y)\delta_{n,-n'} - n(-y)\delta_{n,n'}]\}M_n,$$

where $y = U/2$, $S = 1/2$ is the spin, ω_m is a bosonic Matsubara frequency, ν_n, $\nu_{n'}$ are fermionic Matsubara frequencies, $n(y)$ is the Fermi function, and

$$M_n = \frac{1}{i\nu_n - y} - \frac{1}{i\nu_n + y}.$$

By summing over all fermionic frequencies we have

$$\chi_A(\omega_m) = \frac{1}{\beta^2}\sum_{nn'}[\chi_A(\omega_m)]_{n,n'} = \frac{(g\mu_B S)^2}{k_B T}\frac{e^{\beta U/2}}{1 + e^{\beta U/2}}\delta_{m,0}.$$

In the large βU limit

$$\chi_A(0) \sim \frac{(g\mu_B S)^2}{k_B T}.$$

3. Susceptibility tensor $\chi(\mathbf{q};0)$ in the large U limit

Here we derive an approximate analytic form for the LDA+DMFT magnetic susceptibility, valid in the very large U limit. The static magnetic susceptibility is a tensor with elements $[\chi(\mathbf{q};0)]_{ii',jj'}$, where the indices i, i', j, and j' label the N_c equivalent V sites in the unit cell (cluster). In the case of the systems considered in this work $N_c = 2$; the relevant elements of the static magnetic susceptibility tensor thus built the Hermitian matrix

$$\chi(\mathbf{q};0) = \begin{pmatrix} [\chi(\mathbf{q};0)]_{11,11} & [\chi(\mathbf{q};0)]_{11,22} \\ [\chi(\mathbf{q};0)]_{22,11} & [\chi(\mathbf{q};0)]_{22,22} \end{pmatrix},$$

where by symmetry $[\chi(\mathbf{q};0)]_{11,11} = [\chi(\mathbf{q};0)]_{22,22}$. The $\chi^0(\mathbf{q};0)$ tensor has the same structure. For the latter we can write the elements explicitly

$$[\chi^0(\mathbf{q};0)]_{ii,jj} = -\frac{1}{4\beta}\frac{1}{N_\mathbf{k}}\sum_{n\mathbf{k}\sigma} G^\sigma_{ij}(\mathbf{k}; i\nu_n)G^\sigma_{ji}(\mathbf{k}+\mathbf{q}; i\nu_n),$$

where $G^\sigma_{ij}(\mathbf{k}; i\nu_n)$ is the Green-function matrix. In the large U limit, we can assume that the local self-energy matrix is atomiclike, i.e., that it has the form

$$\Sigma_{ij}(i\nu_n) = \delta_{ij}\frac{r^2U^2}{4}\frac{1}{i\nu_n},$$

where r is a material-specific renormalization factor. By replacing the elements of the self-energy matrix in the Green function with this approximated expression and then performing the Matsubara sums we obtain the elements of the $\chi^0(\mathbf{q};0)$ tensor. Finally, from this we calculate the magnetic coupling matrix

$$J_r(\mathbf{q}) = [\chi^0(\mathbf{q};0)]^{-1} - [\chi^0(0)]^{-1}.$$

We obtain that, in first approximation,

$$J_r^{ij}(\mathbf{q}) \equiv [J_r(\mathbf{q})]_{ii,jj} \sim [J_{\mathrm{SPT}}(\mathbf{q})]_{ii,jj}/2r^2.$$

The elements of the second-order perturbation theory (SPT) exchange coupling tensor are

$$[J_{\mathrm{SPT}}(\mathbf{q})]_{11,11} = 2J_2(\cos q_x + \cos q_y) + 2J_z\cos q_z + 4J_{2z}(\cos q_x + \cos q_y)\cos q_z$$

and

$$[J_{\mathrm{SPT}}(\mathbf{q})]_{11,22} = 4(J_1 + J_{1z}e^{iq_zc})\cos\frac{q_x}{2}\cos\frac{q_y}{2}\,e^{i\mathbf{q}\cdot(\mathbf{R}_1-\mathbf{R}_2)},$$

where $\mathbf{R}_i$ are cluster lattice vectors. To calculate $\chi(\mathbf{q};0)$ we still need the local susceptibility. It turns out that, to a good approximation, the latter is also atomiclike

$$\chi_{ii,jj}(0) = \chi_A(0)\delta_{i,j},$$

and $\chi_A(0) \sim \mu^2_{\mathrm{eff}}/k_BT$. We can now solve analytically the Bethe-Salpeter equation matrix in the local-vertex approximation, and obtain

$$[\chi(\mathbf{q};0)]^{-1} = J_r(\mathbf{q}) + [\chi(0)]^{-1}.$$

The components of the tensor $\chi(\mathbf{q};0)$ are

$$\frac{2[\chi(\mathbf{q};0)]_{ii,jj}}{T\chi_A(0)} \sim \left[\frac{1}{T + \mu^2_{\mathrm{eff}}\left(J_r^{11}(\mathbf{q}) + \widetilde{J}_r^{12}(\mathbf{q})\right)} + \frac{(-1)^{i+j}}{T + \mu^2_{\mathrm{eff}}\left(J_r^{11}(\mathbf{q}) - \widetilde{J}_r^{12}(\mathbf{q})\right)}\right]e^{i\mathbf{q}\cdot(\mathbf{R}_i-\mathbf{R}_j)},$$

where $\widetilde{J}_r^{12}(\mathbf{q}) = \sqrt{J_r^{12}(\mathbf{q})J_r^{21}(\mathbf{q})}$. Finally, we restore the periodicity and obtain the static lattice magnetic susceptibility

$$\chi(\mathbf{q};0) = \frac{1}{2}\sum_{ij}^{N_c}[\chi(\mathbf{q};0)]_{ii,jj}e^{-i\mathbf{q}\cdot(\mathbf{R}_i-\mathbf{R}_j)} \sim \frac{\mu^2_{\mathrm{eff}}}{T - T_\mathbf{q}},$$

where $T_\mathbf{q} = -\mu^2_{\mathrm{eff}}[J_r^{11}(\mathbf{q}) + \widetilde{J}_r^{12}(\mathbf{q})]$.

[1] Edited by C. Lacroix, P. Mendels, and F. Mila, *Introduction to Frustrated Magnetism*, Springer Series in Solid State Science, Vol. 164 (Springer, Berlin, 2011).

[2] R. Melzi, P. Carretta, A. Lascialfari, M. Mambrini, M. Troyer, P. Millet, and F. Mila, Phys. Rev. Lett. **85**, 1318 (2000).

[3] R. Melzi, S. Aldrovandi, F. Tedoldi, P. Carretta, P. Millet, and F. Mila, Phys. Rev. B **64**, 024409 (2001).

[4] P. Carretta, N. Papinutto, C. B. Azzoni, M. C. Mozzati, E. Pavarini, S. Gonthier, and P. Millet, Phys. Rev. B **66**, 094420 (2002).

[5] H. Rosner, R. R. P. Singh, W. H. Zheng, J. Oitmaa, and W. E. Pickett, Phys. Rev. B **67**, 014416 (2003).
[6] H. J. Schulz, T. A. L. Ziman, and D. Poilblanc, J. Phys. I (France) **6**, 675 (1996).
[7] L. Siurakshina, D. Ihle, and R. Hayn, Phys. Rev. B **64**, 104406 (2001).
[8] L. Spanu and A. Parola, Phys. Rev. B **72**, 174418 (2005).
[9] J. Reuther, P. Wölfle, R. Darradi, W. Brenig, M. Arlego, and J. Richter, Phys. Rev. B **83**, 064416 (2011).
[10] H.-Y. Wang, Phys. Rev. B **86**, 144411 (2012).
[11] Y. Yamashita and K. Ueda, Phys. Rev. Lett. **85**, 4960 (2000).
[12] O. Tchernyshyov, R. Moessner, and S. L. Sondhi, Phys. Rev. Lett. **88**, 067203 (2002).
[13] F. Becca and F. Mila, Phys. Rev. Lett. **89**, 037204 (2002).
[14] F. Duc, S. Gonthier, M. Brunelli, and J. C. Trombe, Solid State Chem. **179**, 3591 (2006).
[15] H. Kageyama, T. Kitano, N. Oba, M. Nishi, S. Nagai, K. Hirota, L. Viciu, J. B. Wiley. J. Yasuda. Y. Baba, Y. Ajiro, and K. Yoshimura, J. Phys. Soc. Jpn. **74**, 1702 (2005).
[16] A. A. Tsirlin and H. Rosner, Phys. Rev. B **79**, 214417 (2009).
[17] N. Read and S. Sachdev, Phys. Rev. Lett. **66**, 1773 (1991).
[18] M. Zema, S. C. Tarantino, P. Ghigna, and G. Montagna, Z. Kristallogr. **222**, 350 (2007).
[19] P. Chandra, P. Coleman, and A. I. Larkin, Phys. Rev. Lett. **64**, 88 (1990).
[20] H. Rosner, R. R. P. Singh, W. H. Zheng, J. Oitmaa, S.-L. Drechsler, and W. E. Pickett, Phys. Rev. Lett. **88**, 186405 (2002).
[21] E. Pavarini, S. C. Tarantino, T. B. Ballaran, M. Zema, P. Ghigna, and P. Carretta, Phys. Rev. B **77**, 014425 (2008).
[22] A. Bombardi, J. Rodriguez-Carvajal, S. Di Matteo, F. de Bergevin, L. Paolasini, P. Carretta, P. Millet, and R. Caciuffo, Phys. Rev. Lett. **93**, 027202 (2004).
[23] A. Bombardi, L. C. Chapon, I. Margiolaki, C. Mazzoli, S. Gonthier, F. Duc, and P. G. Radaelli, Phys. Rev. B **71**, 220406 (2005).
[24] Remarkably, the low-energy electronic structure of layered vanadates has several similarities with that of high-temperature superconducting cuprates (HTSCs) [26]. Although the chemical bond in the xy band of the first is very different with respect to the $x^2 - y^2$ band of the latter—in layered vanadates the pyramids do not share oxygens and are well separated by either MoO_4 or by SiO_4 polyhedra—based on their two dimensionality and their low-energy electronic structure, layered vanadates could in the future even turn out to be interesting candidates for engineering [26,27] two-dimensional superconductors or systems with other nonconventional properties.
[25] The effective local spin S is obtained from the expectation value of the local spin-spin correlation function, i.e., from $\langle S_z S_z \rangle = S(S+1)/3$; the latter yields the high-temperature tail of the local susceptibility $\chi_{zz}(T) \propto \langle S_z S_z \rangle / T$; hence, S is different from $m = g\mu_B \langle S_z \rangle$, which is finite only for temperatures $T < T_N$.
[26] E. Pavarini, I. Dasgupta, T. Saha-Dasgupta, O. Jepsen, and O. K. Andersen, Phys. Rev. Lett. **87**, 047003 (2001).
[27] P. Hansmann, X. Yang, A. Toschi, G. Khaliullin, O. K. Andersen, and K. Held, Phys. Rev. Lett. **103**, 016401 (2009).
[28] Edited by E. Pavarini, E. Koch, D. Vollhardt, and A. Lichtenstein, *The LDA+DMFT Approach to Strongly Correlated Materials* (Verlag des Forschungszentrum, Jülich, 2011), Reihe Modeling and Simulation, Vol. 1. Open access at: http://www.cond-mat.de/events/correl.html and http://hdl.handle.net/2128/4467.
[29] E. Pavarini, S. Biermann, A. Poteryaev, and A. I. Lichtenstein, A. Georges, and O. K. Andersen, Phys. Rev. Lett. **92**, 176403 (2004); E. Pavarini, A. Yamasaki, J. Nuss, and O. K. Andersen, New J. Phys. **7**, 188 (2005); M. De Raychaudhury, E. Pavarini, and O. K. Andersen, Phys. Rev. Lett. **99**, 126402 (2007).
[30] A. Georges, G. Kotliar, W. Krauth, and M. J. Rozenberg, Rev. Mod. Phys. **68**, 13 (1996).
[31] J. E. Hirsch and R. M. Fye, Phys. Rev. Lett. **56**, 2521 (1986).
[32] E. Gull, A. J. Millis, A. I. Lichtenstein, A. N. Rubtsov, M. Troyer, and P. Werner, Rev. Mod. Phys. **83**, 349 (2011).
[33] A. Flesch, E. Gorelov, E. Koch, and E. Pavarini, Phys. Rev. B **87**, 195141 (2013).
[34] Edited by E. Pavarini, E. Koch, D. Vollhardt, and A. I. Lichtenstein, *DMFT at 25: Infinite Dimensions* (Verlag des Forschungszentrum, Jülich, 2014), Reihe Modeling and Simulation, Vol. 4. Open access at: http://www.cond-mat.de/events/correl.html or at http://juser.fz-juelich.de/record/155829.
[35] M. Jarrell, Phys. Rev. Lett. **69**, 168 (1992).
[36] S. Chakravarty, B. I. Halperin, and D. R. Nelson, Phys. Rev. Lett. **60**, 1057 (1988).
[37] Notice that a small error in the relative weights of $2J_{1z}$ and $J_z + 4J_{2z}$ affects little the Curie-Weiss temperature, which averages over all couplings.
[38] G. Dahlquist and A. Björck, *Numerical Methods in Scientific Computing* (Society for Industrial and Applied Mathematics, Philadelphia, 2007), Vol. 1.
[39] The Filon-trapezoidal method was also used in O. Gunnarsson, G. Sangiovanni, A. Valli, and M. W. Haverkort, Phys. Rev. B **82**, 233104 (2010).